EurJIC European Journal of Inorganic Chemistry
ChemPubSoc Europe
FULL PAPER

DOI:10.1002/ejic.201500310

Magnetofluorescent Nanoaggregates Incorporating Terbium(III) Complexes as Potential Bimodal Agents for Magnetic Resonance and Optical Imaging

CLUSTER ISSUE

Michael Harris,[a] Sophie Carron,[a] Luce Vander Elst,[b,c] Sophie Laurent,[b,c] and Tatjana N. Parac-Vogt*[a]

Keywords: Nanostructures / Nanoaggregates / Micelles / Imaging agents / Bimodal imaging / Lanthanides / Carboxylate ligands

Terbium(III) ions were coordinated to two diethylenetriaminepentaacetic acid (DTPA) amphiphilic bisamide ligands, and the complexes were assembled into micellar nanoaggregates. The magnetic and optical properties of the resulting nanoaggregates were examined in detail. Upon excitation into the ligand levels at 265 nm, the complexes show characteristic Tb^{III} emission at 546 nm with quantum yields of up to 7.6 %. Nuclear magnetic relaxation dispersion (NMRD) measurements have shown that the transverse relaxivity r_2 at 500 MHz and 310 K reaches a maximum value of 9.4 s^{-1} mM^{-1}. The efficient T_2 relaxivity at high magnetic field strengths is sustained by the increased rotational correlation time of the nanoaggregates and high magnetic moment of the terbium ion.

Introduction

Powerful in vivo techniques such as magnetic resonance imaging (MRI), positron emission tomography (PET), fluorescence imaging and bioluminescence are indispensable in clinical diagnostics. As each imaging technique has its own strengths and weaknesses, approaches that combine different, complementary techniques could overcome the inherent limitations associated with one individual technique. Although MRI is ideal for whole-body images owing to its good spatial resolution, large concentrations of Gd^{III}-based contrast agents are required owing to its rather low sensitivity.[1] On the other hand, luminescence-based imaging can provide high-resolution images, but this technique is only suitable for thin tissue samples because of the low optical transparency of biological tissue.[2]

The current contrast agents (CAs) used in magnetic resonance imaging (MRI) are based on gadolinium(III) complexes with diethylenetriaminepentaacetic acid (DTPA) or 1,4,7,10-tetraazacyclododecane-1,4,7,10-tetraacetic acid (DOTA), which shorten the longitudinal relaxation time (T_1) of water protons and produce a positive contrast but suffer from dramatic loss of efficiency at high magnetic fields.[3]

Alternatively, iron oxide nanoparticles can accelerate the transverse relaxation time of water protons (T_2) to produce a negative contrast.[4] Decreasing the molecular tumbling rate of the Gd^{III} complex through the conjugation of chelates to polymers or dendrimers,[5] noncovalent interactions with human serum albumin[6] or incorporation into supramolecular micelles or liposomes[7] has been frequently used to increase the relaxation performance of contrast agents, especially for high-magnetic-field applications.

In a recent effort to enhance the imaging performance of CAs, probes combining MRI and luminescence properties have been synthesized to combine good resolution with high sensitivity and, thereby, allow the investigation of samples in exquisite detail.[8] The attachment of DTPA and DOTA to several organic dyes[9] and transition metal complexes[10] have been investigated, and their bimodal applications have been exploited. The design and characterization of fluorescent liposomes[11] and nanoparticles to enhance the longitudinal[12] or transverse relaxation times[13] have also been reported. The use of bioconjugates led to significant improvements of MRI and optical properties; however, practical applications are limited by the short luminescence lifetimes (100–300 ns), small Stokes shifts and poor resistance to photobleaching of the organic fluorophores. In a different approach, transition metal complexes have been linked to DTPA or DOTA to produce luminescent

[a] Department of Chemistry, KU Leuven, Celestijnenlaan 200F, 3001 Leuven, Belgium
E-mail: tatjana.vogt@chem.kuleuven.be
http://chem.kuleuven.be/lbc/
[b] Department of General, Organic and Biomedical Chemistry, NMR and Molecular Imaging Laboratory, University of Mons, 7000 Mons, Belgium
E-mail: luce.vanderelst@umons.be
[c] CMMI – Center for Microscopy and Molecular Imaging, 6041 Gosselies, Belgium
Supporting information for this article is available on the WWW under http://dx.doi.org/10.1002/ejic.201500310.

CAs.[10a,10b,14] However, in terms of their luminescence properties, lanthanides have several advantages as they can exhibit excited-state lifetimes in the range of milliseconds and, thereby, remove the problem of short-lifetime autofluorescence. In addition, they have sharply spiked emission spectra, a large energy difference between their emission bands, and absorption bands of coordinated sensitizers, which often results in impressive luminescence. However, as gadolinium(III) ions are not luminescent, the creation of a bimodal CA containing the gadolinium(III) centre needed to produce an MRI signal and another luminescent lanthanide centre for the optical signal is challenging owing to the very similar coordination properties across the lanthanide series. We recently reported a successful strategy for the creation of a heteropolymetallic lanthanide complex[14a] with selectively incorporated gadolinium(III) and europium(III) ions. The multistep synthetic procedure resulted in a metallostar complex with favourable luminescence and relaxometric properties. In another approach, the incorporation of amphiphilic gadolinium(III) complexes with europium(III) complexes into micelles resulted in magnetofluorescent nanoaggregates, in which the relaxivity and luminescence intensity could be tuned by changing the ratio of the amphiphilic gadolinium(III) and europium(III) complexes.[15]

However, the field of bimodal imaging with one single chelated Ln^{III} ion has been very scarcely explored. We recently reported a new approach towards bimodal contrast agents based on a single Ln^{III} ion by exploiting the unique properties of Dy^{III} and Tb^{III} ions.[16] Dy^{III} and Tb^{III} complexes show strong luminescence owing to the effective shielding of their valence electrons and are, therefore, characterized by sharp emission lines, which make them appropriate for optical imaging (OI) applications. In addition, owing to the large magnetic moments of Dy^{III} and Tb^{III} ions, their complexes exhibit large T_2 relaxivities at higher magnetic fields. This is a very interesting property as modern MRI instruments are progressively using higher magnetic field strengths at which traditional Gd^{III} T_1 positive contrast agents such as Gd-DTPA and Gd-DOTA suffer from dramatic decreases in performance.[17] Furthermore, a significant increase of T_2 relaxivity is predicted if the molecular volume and rotational correlation time (τ_C) of CAs increase. A convenient approach to increase the size of the CAs is to incorporate them into biocompatible nanoaggregates. The incorporation of amphiphilic Dy^{III} and Tb^{III} complexes into mixed micelles indeed resulted in assemblies that showed large transverse relaxivities at magnetic fields of 300–500 MHz.[16] A comparison between Dy^{III} and Tb^{III} nanoaggregates revealed that the Tb^{III} nanoaggregates hold more potential as bimodal probes because of their larger quantum yields and comparably efficient transverse relaxivity at high fields. Therefore, in this study, we further explore the potential of nanoaggregates based on Tb^{III} complexes as potential CAs for MRI and optical imaging and report two new Tb^{III} complexes based on amphiphilic DTPA ligands, which were synthesized by a facile route. The ligands were derivatized with *p*-alkylphenylamides, which can be excited at a wavelength of 265 nm and upon energy transfer to the Tb^{III} centre result in observable luminescence. A new procedure to create smaller micelles of approximately 10 nm has been developed to produce CAs that are potentially more biocompatible owing to their possible easier excretion. The relaxation and luminescence efficiency of the resulting nanoaggregates have been investigated in detail, and their potential as CAs for MRI and optical imaging has been discussed.

Results and Discussion

Synthesis of Ligands, Complexes and Aggregates

Two DTPA bisamide derivatives with long hydrophobic side chains were synthesized according a literature procedure.[18] The synthetic pathway and the obtained ligands Tb-DTPA-BC_{12}PheA and Tb-DTPA-BC_{14}PheA are presented in Scheme 1. All of the ligands were characterized by nuclear magnetic resonance spectroscopy, mass spectrometry, and IR spectroscopy.

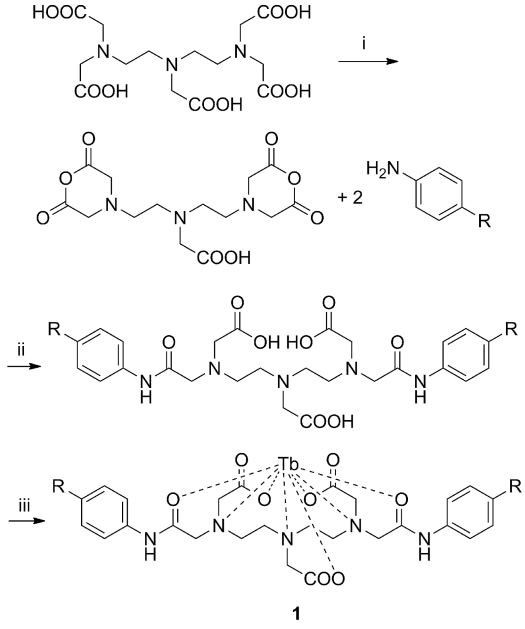

Scheme 1. (i) Acetic anhydride (2 equiv.), pyridine (4 equiv.), 65 °C, 1 h. (ii) *N*,*N*-dimethylformamide (DMF), $CHCl_3$, 50 °C, 8 h. (iii) Pyridine, 70 °C, 3 h. **1**: Tb-DTPA-BC_{12}PhenA or Tb-DTPA-BC_{14}PhenA with coordinated water molecule omitted; R = C_{12} or C_{14} alkyl chain.

The two ligands were coordinated to Tb^{III} ions in pyridine by a slightly modified procedure.[17] The DTPA chelator was dissolved in pyridine, and a solution of hydrated $TbCl_3$ (1.1 equiv.) in water was added. The solution was mixed for 3 h, and the solvents were evaporated. The solid product was suspended in acetone, collected by filtration, washed with acetone, acetone/water (50:50) and again with acetone, and then dried in vacuo. The absence of free lanthanide ions was verified by the addition of an arsenazo(III) indicator solution.[19] The complex formation was established by mass spectrometry (Figures S1 and S2

in the Supporting Information), IR spectroscopy, and total reflection X-ray fluorescence (TXRF) analysis.

The lanthanide complexes of DTPA-BC_{12}PhenA and DTPA-BC_{14}PhenA consist of a hydrophilic centre and two hydrophobic tails with a phenyl ring and a chain of 12 or 14 carbon atoms. The amphiphilic nature permits them to be incorporated into mixed micelles to create slowly tumbling supramolecular structures with limited local motion of the lanthanide complexes. Variation of the ratio of surfactant to phospholipid and Tb^{III} complex was investigated to gain control over the nanoaggregate formation. We observed that increasing the surfactant to 50 mol-% or greater resulted in small nanoaggregates. The nanoaggregates were formed by mixing 1 equiv. of the Ln complex of interest with 12 equiv. of phospholipid (DPPC) and 6.5 equiv. of surfactant (Tween 80®). Photon correlation spectroscopy measurements showed two different size distribution profiles for the C_{12} and C_{14} alkyl chain systems (Figures S3 and S4). The C_{12} system had a narrower size distribution than the C_{14} system, possibly because of the disruption of the DPPC packing in the micelles with the C_{14} system. This has allowed completely transparent nanoaggregate solutions with distribution maxima at 9 nm for Tb-DTPA-BC_{12}PheA and 11 nm for Tb-DTPA-BC_{14}PheA. Furthermore, in the C_{12} distribution, a small peak at ca. 1 nm was observed and identified to most likely originate from micelles formed by surfactant Tween 80® alone.

Photophysical Properties

Owing to the $\pi \rightarrow \pi^*$ transitions of the ligands, the terbium complexes display well-defined absorption bands (Figure 1). As shown in Figure 1, a ligand-centred band in the range λ = 220–300 nm with a maximum at $\lambda \approx$ 240–260 is observed in the absorption spectrum of the supramolecular structures corresponding to the ligand electronic transitions. The excitation spectrum of Tb-DTPA-BC_{12}PhenA (Figure 2) shows a small shoulder at $\lambda \approx$ 300 nm, which could be caused by the varied incorporation of the complex into the DPPC micelles. For both complexes, a wavelength of 265 nm remains the most efficient for energy transfer to the Tb^{III} ions.

The emission spectra of the micelles display sharp emission bands attributed to the $^5D_4 \rightarrow {}^7F_J$ (J = 9–3) transitions of the Tb^{III} ions upon excitation at 265 nm (Figure 3). The efficient energy transfer from the ligand to lanthanide ion is maintained as little ligand-centred emission is detected.

The luminescence decays were measured in both H_2O and D_2O, and the monoexponential fit indicates the presence of only one luminescent lanthanide species in the micellar structures. The luminescence lifetimes in H_2O are 1.8 and 2.1 ms for the micelles consisting of Tb-DTPA-BC_{12}PheA and Tb-DTPA-BC_{14}PheA, respectively. In D_2O, luminescence lifetimes of up to 2.6 and 2.7 ms were obtained for Tb-DTPA-BC_{12}PheA and Tb-DTPA-BC_{14}PheA, respectively. Within the uncertainty of the luminescence method, the phenomenological Equation (1) for Tb^{III} polyaminocarboxylate systems[20] was employed to determine the number of coordinated water molecules q with an accuracy of ±0.2–0.3:

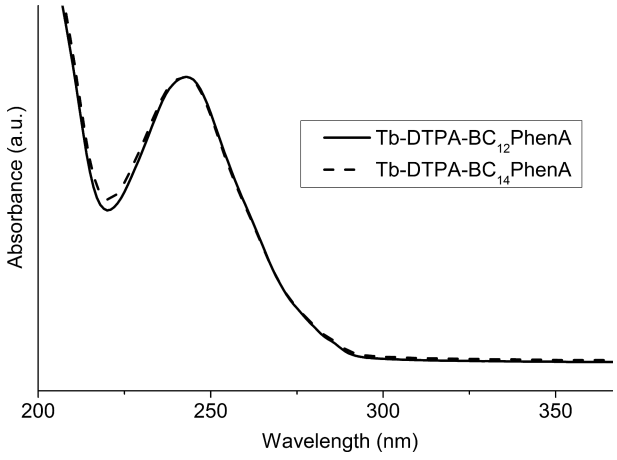

Figure 1. Normalized absorbance spectra of Tb^{III} complexes in water (pH 7.4, 1 wt.-%, 298 K).

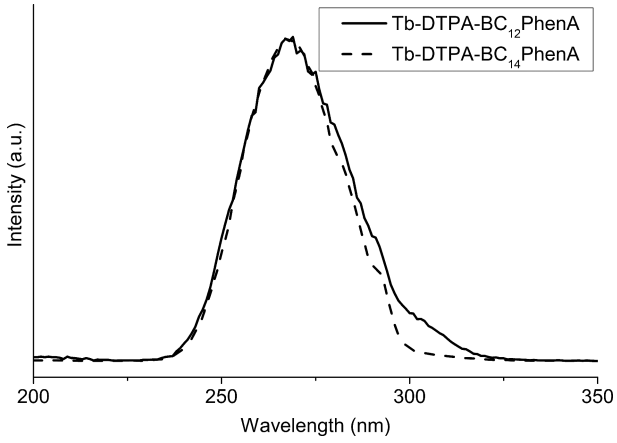

Figure 2. Corrected and normalized excitation spectra of Tb^{III} complexes in water (pH 7.4, 1 wt.-%, 298 K). Emission wavelength 546 nm.

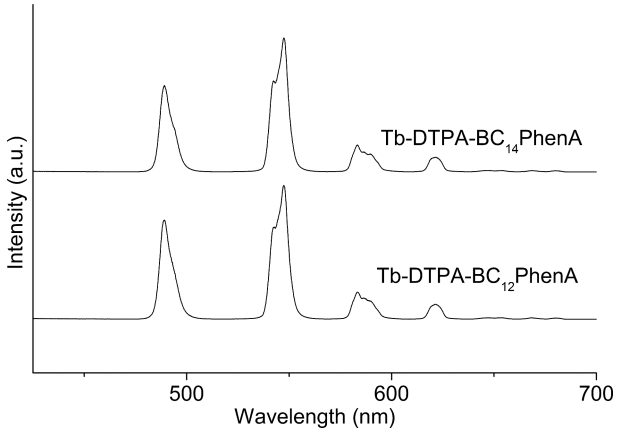

Figure 3. Corrected and normalized emission spectra of Tb^{III} complexes in water (pH 7.4, 1 wt.-%, 298 K). Excitation wavelength 265 nm.

$$q_{Tb}\ (H_2O) = 5.0(\Delta k_{obs} - 0.06) \quad (1)$$

$\Delta k_{obs} = 1/\tau_{H2O} - 1/\tau_{D2O}$ is expressed in ms^{-1}. According to Equation (1), q values of 0.4 and 0.3 were obtained for Tb-DTPA-BC_{12}PheA and Tb-DTPA-BC_{14}PheA, respectively. According to Scheme 1, the Tb^{III} complex should have one water ligand in its first coordination sphere. However, the nonionic surfactant Tween 80® at the periphery of the assembled structures is able to form hydrogen bonds with H_2O and act as a competitor in lanthanide coordination, which results in a value of less than 1. As a consequence, less nonradiative deactivation due to O–H vibrations will lead to longer luminescence lifetimes and, consequently, to a reduced q number in the phenomenological Equation (1).[21]

The Tb^{III} luminescence quantum yields were determined by excitation at 265 nm into the ligand levels. The values were calculated to be 7.6% for both complexes (Table 1).

Table 1. Photophysical data for the Tb^{III} complexes in water (pH 7.4, 1 wt.-%) at 298 K.

	τ H_2O [ms]	τ D_2O [ms]	q	Q^L_{Tb}[a] [%]
DTPA-BC_{12}PhenA	1.8(1)	2.4(1)	0.4	7.6
DTPA-BC_{14}PhenA	2.1(1)	2.7(1)	0.3	7.6

[a] Estimated relative errors $Q^L_{Tb} \pm 10\%$. Quantum yields relative to rhodamine 101 in EtOH.

Relaxometric Studies

Proton Longitudinal Relaxation Rate

The enhancement of the relaxation rate by 1 mM of the Tb^{III} compound determines the proton longitudinal relaxivity (r_1). In Figure 4, the proton longitudinal relaxivities of the two compounds at 20, 60, 300, and 500 MHz are depicted. The profiles of the two compounds follow the same trend. At low magnetic fields (20–60 MHz), low r_1 values of 0.10–0.11 $mM^{-1}s^{-1}$ were obtained. At higher magnetic fields (300–500 MHz), a slight increase of r_1 to 0.12–0.15 $mM^{-1}s^{-1}$ was observed. The variation between the complexes corresponds to the variation of the q values, as has been previously observed with Tb-DOTA complexes.[16b]

Both inner- ($1/T_1^{is}$) and outer-sphere ($1/T_1^{os}$) contributions to the proton longitudinal relaxation rate are defined by the sum of dipolar ($1/T_1^{DD}$) and Curie ($1/T_1^{C}$) contributions. At low magnetic fields, the longitudinal relaxation rate is mainly modulated by the dipolar interactions between the water protons and the static magnetic moments of the electrons of the Tb^{III} centres and is highly dependent on the electronic relaxation time τ_S.[22] Those findings explain the low r_1 values in this region, as Tb^{III} ions are characterized by very short τ_S values (ca. 0.5 ps).[22a,23] At high magnetic fields, the Curie inner- and outer-sphere contributions become more significant. These terms are modulated by the rotational correlation time of the compound τ_R and the translational correlation time τ_D; τ_D equals a^2/D, in which a is the distance of the closest approach between the water protons and the paramagnetic centre, and D is the relative diffusion constant of the water molecules. Thus, the proton longitudinal relaxivity will increase slightly at higher fields.

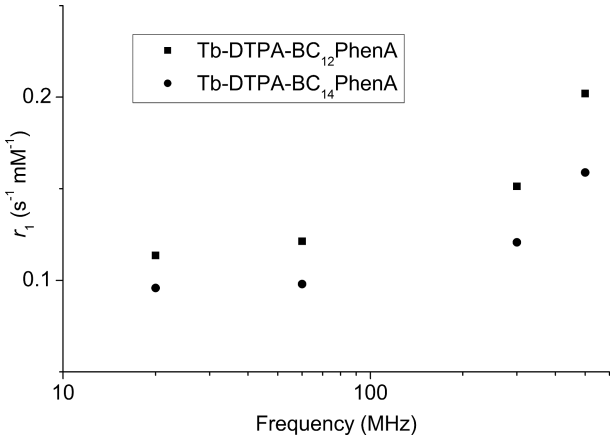

Figure 4. Proton longitudinal relaxivity of the micelles versus proton Larmor frequency at 310 K.

Proton Transverse Relaxation Tate

The T_2 enhancements at 20, 60, 300 and 500 MHz by the complexes are depicted in Figure 5. At the proton Larmor frequency of 20 MHz, the transverse relaxivities for the complexes are slightly higher in comparison to the longitudinal values (r_2 = 0.17 $mM^{-1}s^{-1}$). This increase is due to the relative large values of τ_M and $\Delta\omega_M$. At higher magnetic fields (ν_o > 100 MHz), r_2 increases. Although the transverse relaxivity depends on the square of the magnetic field, r_2 shows a strong reliance on the τ_M value as the external magnetic field increases. In that particular case, it is important that the chemical shift difference between coordinated and bulk water ($\Delta\omega_M$) remains low relative to the water exchange to avoid limitation by τ_M.[22a] The chemical shift of the coordinated water molecule is proportional to the magnetic field and is the sum of contact and pseudocontact terms.

The fitting of the data was performed by using the equations defining the inner- and outer-sphere contributions as described by Vander Elst et al.[22a] The inner-sphere contributions depend on the ratio [Tb complex]/[water], the value of q, the water residence time τ_M and the transverse relaxation rate of the coordinated water molecule $1/T_{2M}$. The latter factor results from dipolar, dipolar Curie, and Curie contact contributions. The correlation time τ_C modulates the dipolar interaction and is related to τ_R, τ_S and τ_M through $\tau_C^{-1} = \tau_R^{-1} + \tau_S^{-1} + \tau_M^{-1}$, whereas the Curie contribution is modulated by τ_{CC}, which is defined as $\tau_{CC}^{-1} = \tau_R^{-1} + \tau_M^{-1}$. During the fitting procedure, the parameters q = bound water molecules(s) as determined by luminescence lifetimes, r = 0.31 nm, a = 0.36 nm, $D = 3.3 \times 10^{-9}\ m^2 s^{-1}$

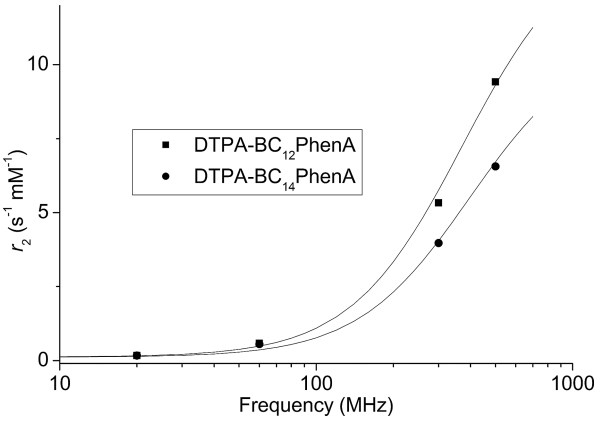

Figure 5. Proton transverse relaxivity of the micelles versus proton Larmor frequency at 310 K. The lines represent the fitted data. The concentration of DTPA-BC$_{12}$Phen A was 6.38 mM, and that of DTPA-BC$_{14}$Phen A C14 was 6.03 mM.

and τ_R = 1 ns were fixed. The parameters τ_S, τ_M and $\Delta\omega_M$ were extracted from the fit and are listed in Table 2 but should only be considered as estimates as the fit is only over four points.

Table 2. Values of τ_S, τ_M and $\Delta\omega_M$ obtained by fitting the ^{1}H r_2 data of the Tb^{III} complexes at 310 K.

	τ_s [ps]	τ_M [ns]	$\Delta\omega_M$ [10^5 rad s^{-1} T^{-1}]
DTPA-BC$_{12}$PhenA	0.25	500	2.3
DTPA-BC$_{14}$PhenA	0.25	500	2.1

The τ_S values were 0.25 ps. The fit of the proton nuclear magnetic relaxation dispersion (NMRD) profiles of the micelles indicates that there is little difference between the C_{12} and C_{14} complexes. The slow molecular motion leads to transverse relaxivities of 9.4 and 6.6 s^{-1} mM^{-1} at 500 MHz and 310 K for Tb-DTPA-BC$_{12}$PheA and Tb-DTPA-BC$_{14}$PheA, respectively. The slight variation of the number of coordinated water molecules (0.4 to 0.3) shows that the Tb-DTPA-BC$_{12}$PheA micelles with the greatest q value are the most efficient negative contrast agent. The performances of the compounds as efficient r_2 agents are enforced by the high magnetic moment of the terbium ion (μ = 9.81 μ_B), the presence of water molecules in the first coordination sphere and long rotational correlation time.[22b] Furthermore, DPPC forms micelles of 50 phospholipid molecules[24] in which the Tb^{III} load would most likely be four molecules per micelle.

As tissues display a shorter T_2 than T_1, contrast agents with significant r_2/r_1 ratios can be beneficial through the use of appropriate pulse sequences in clinical applications. In Figure 6, the r_2/r_1 ratios are depicted. The ratio increases for both complexes with increasing magnetic field strength. The largest ratio of r_2/r_1 is observed for Tb-DTPA-BC$_{12}$PheA; however, the two complexes show very similar behaviour.

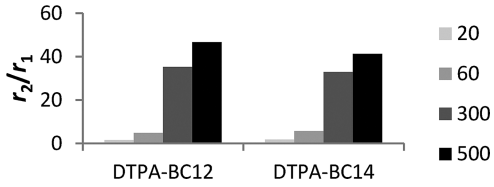

Figure 6. Ratios of proton transverse versus longitudinal relaxivity at 20, 60, 300 and 500 MHz for the Tb^{III} complexes at 310 K.

Conclusions

The amphiphilic terbium(III) complexes built into mixed micelles reported in this study show magnetic and optical properties that make them potential candidates for magnetic resonance and optical imaging. The micelles showed long luminescence lifetimes in H_2O at the emission wavelength of 546 nm and high quantum yields of up to 7.6%. The complexes also exhibit transverse relaxivities r_2 of close to 10 s^{-1} mM^{-1} at 500 MHz and 310 K. In comparison with previously reported Dy^{III}-DTPA micelle complexes, the Tb^{III} complexes provides a large increase in luminescence quantum yields. Additionally, in comparison with the values for previously reported Dy^{III}-DTPA micelle complexes,[16a] a decrease in r_2 has been observed, which could mainly result from a significant decrease in the nanoaggregate sizes for the Tb^{III} complexes. Smaller micelles are advantageous for biocompatibility and elimination from the body, and in this work we created monodisperse nanoaggregates; the C_{12} alkyl system showed the narrowest distribution in the 9 nm range. In comparison with our recently reported Tb-DOTA complexes,[16b] the DTPA complexes show slightly less efficient T_2 relaxivity. This is most likely a consequence of decreased water exchange kinetics and a lower number of bound water molecules in the DTPA complexes. However, the advantage of the complexes reported in this work is their more facile synthetic route. The excitation at 265 nm could be overcome by further optimization of the complexes by using different chromophores. This may lead to further improvements to the optical properties and establish Tb^{III} complexes as a class of potential candidates for magnetic resonance and optical imaging.

Experimental Section

Materials: Reagents and solvents were obtained from Sigma–Aldrich (Bornem, Belgium), Acros Organics (Geel, Belgium), ChemLab (Zedelgem, Belgium), Matrix Scientific (Columbia, USA) and BDH Prolabo (Leuven, Belgium) and were used without further purification. Terbium(III) chloride hexahydrate was obtained from Sigma–Aldrich (Bornem, Belgium).

Instrumentation: ^{1}H NMR spectra were recorded by using a Bruker Avance 300 spectrometer (Bruker, Karlsruhe, Germany) operating at 300 MHz.

IR spectra were recorded by using a Bruker Vertex 70 FTIR spectrometer (Bruker, Ettlingen, Germany).

Mass spectra were obtained by using a Thermo Finnigan LCQ Advantage mass spectrometer. Samples for the mass spectrometry

were prepared by dissolving the product (2 mg) in methanol (1 mL), and then adding this solution (200 μL) to a water/methanol mixture (50:50, 800 μL). The resulting solution was injected at a flow rate of 5 μL min^{-1}.

The TXRF measurements were performed with a Bruker S2 Picofox spectrometer (Bruker, Berlin, Germany) with a molybdenum source. Terbium(III) solutions of approximately 1000 ppm in milli-Q water were prepared and these solutions (500 μL) were mixed with a 1000 ppm Chem-Lab gallium standard solution (500 μL, 1000 μg/mL, 2–5% HNO_3). This mixture with similar Tb^{III} and Ga^{III} concentrations was placed on a Bruker AXS quartz glass sample plate for measurement.

The solutions were dispersed with a 180-W Bandelin Sonorex RK 510 H sonicator equipped with a thermostatic heating bath.

The absorption spectra were recorded with a Varian Cary 5000 spectrophotometer with freshly prepared aqueous solutions in quartz Suprasil cells (115F-QS) with an optical pathlength of 1 cm.

The emission spectra and luminescence decays of the Tb^{III} micellar complexes were recorded with an Edinburgh Instruments FS920 steady-state spectrofluorimeter. This instrument was equipped with a 450W xenon arc lamp, a high-energy microsecond flashlamp (mF900H) and an extended red-sensitive photomultiplier (185–1010 nm, Hamamatsu R 2658P). All spectra are corrected for the instrumental functions. The luminescence decays were determined under ligand excitation (265 nm) with the emission of the $^5D_4 \rightarrow 7F_J$ (J = 9–3) transition of the Tb^{III} complexes monitored. The luminescence decays were analyzed by using Edinburgh software; the lifetimes are averages of at least three measurements. The quantum yields were determined by a comparative method with a standard reference; the estimated experimental errors for the quantum yield determinations are ±10%. Rhodamine 101 (Sigma) in ethanol (Q = 100%) was used as a standard for the complexes. Solutions with concentrations of ca. 10^{-5} M were prepared to obtain an optical density lower than 0.05 at the excitation wavelength.

Relaxometry: ^1H T_1 and T_2 measurements were performed at 310 K and 0.47, 1.41, 7.05 and 11.75 T with Bruker Minispec mq-20, mq-60, Avance-300 and Avance-500 instruments, respectively. The T_1 values were measured by using the inversion-recovery sequence, and the T_2 values were obtained by using the CMPG sequence. The echo time was set to 1 ms. The diamagnetic contribution was the contribution of pure water.

Dynamic Light Scattering Measurements: Photon correlation spectroscopy was performed at room temperature with a BIC multiangle laser light-scattering system with a 90° scattering angle (Brookhaven Instruments Corporation, Holtsville, USA). The intensity-weighted micellar diameter was measured for 0.1 wt.-% diluted suspensions in Milli-Q water, sonicated for 15 min, passed through a 200 nm polytetrafluoroethylene (PTFE) filter before analysis and calculated by a non-negatively constrained least-squares (multiple pass) routine.

Synthesis: DTPA bisanhydride and DTPA ligands were synthesized as described previously.[16a]

DTPA-BC_{12}PhenA: Yield 1.05 g, 62%. ^1H NMR {300 MHz, [D_5]-pyridine, 25 °C, tetramethylsilane TMS): δ = 0.88 [t, 6 H, $CH_3(CH_2)_9CH_2CH_2Ar$], 1.26 [m, 36 H, $CH_3(CH_2)_9CH_2CH_2Ar$], 1.58 [m, 4 H, $CH_3(CH_2)_9CH_2CH_2Ar$], 2.55 [t, 4 H, $CH_3(CH_2)_9CH_2CH_2Ar$], 3.19 (t, 8 H, NCH_2CH_2N), 3.82, 3.84, 3.86 [t, 10 H, $NCH_2C(O)$], 7.22, 7.26 ppm (d, 4 H, under solvent signal, phenyl C*H*), 8.14, 8.17 (d, 4 H, phenyl C*H*), 10.68 ppm (s, 2 H, amide N*H*). ESI-MS (+): m/z = 881.2 [M + H]$^+$, 903.0 [M + Na]$^+$.

DTPA-BC_{14}PhenA: Yield 1.2 g, 91%. ^1H NMR (300 MHz, [D_5]-pyridine, 25 °C, TMS): δ = 0.88 [t, 6 H, $CH_3(CH_2)_{11}CH_2CH_2Ar$], 1.26 [m, 44 H, $CH_3(CH_2)_{11}CH_2CH_2Ar$], 1.59 [m, 4 H, $CH_3(CH_2)_9CH_2CH_2Ar$], 2.56 [t, 4 H, $CH_3(CH_2)_9CH_2CH_2Ar$], 3.19 (t, 8 H, NCH_2CH_2N), 3.82, 3.84, 3.86 [t, 10 H, $NCH_2C(O)$], 7.22, 7.26 ppm (d, 4 H, under solvent signal, phenyl C*H*), 8.14, 8.17 (d, 4 H, phenyl C*H*), 10.68 ppm (s, 2 H, amide N*H*). ESI-MS (+): m/z = 937.8 [M + H]$^+$, 958.9 [M + Na]$^+$.

Terbium(III) DTPA-BC_{12}PhenA and DTPA-BC_{14}PhenA Complexes: The ligand (0.1 g, ±0.1 mmol, 1 equiv.) was dissolved in pyridine (5 mL), and a solution of hydrated $TbCl_3$ hexahydrate salt (0.11 mmol, 1.1 equiv.) in H_2O (0.2 mL) was added. The mixture was heated to 70 °C for 3 h, after which the solvents were evaporated. The crude product was suspended in acetone (10 mL) and filtered through a Büchner funnel. The solid was washed with an acetone/water 50:50 mixture (2× 5 mL) to remove any free Tb^{III} ions, rinsed again with acetone (2× 10 mL) and dried in vacuo. The absence of free lanthanide ions was checked with an arsenazo indicator.

Tb^{III}-DTPA-BC_{12}PhenA: Yield 80%. IR: $\tilde{\nu}_{max}$ = 1596 (COO^- asym. stretch), 1514 (amide II), 1391 cm^{-1} (COO^- sym. stretch). ESI-MS (+): m/z = 1036.8 [M + H]$^+$, 1058.8 [M + Na]$^+$.

Tb^{III}-DTPA-BC_{14}PhenA: Yield 82%. IR: $\tilde{\nu}_{max}$ = 1595 (COO^- asym. stretch), 1514 (amide II), 1392 cm^{-1} (COO^- sym. stretch). ESI-MS (+): m/z = 1092.8[M + H]$^+$, 1116.0[M + Na]$^+$.

Preparation of Micelles: 1,2-Dipalmitoyl-*sn*-glycero-3-phosphocholine (DPPC, 80 mg, 0.109 mmol, 12 equiv.) and the amphiphilic complex (10 mg, ±0.091 mmol, 1 equiv.) were dissolved in a 1:1 chloroform/methanol solution (2 mL). After the evaporation of the solvents from a flask with a septum and a needle fitted in a vacuum oven at 50 °C, the obtained thin film was rehydrated with hot water (2 mL, 70 °C). To improve the solubility, the suspension was sonicated with a 180 W sonicator with a thermostatic bath at 65 °C for 15 min. Polyoxyethylene sorbitan monooleate or Tween 80® (77 mg, 0.06 mmol, 6.5 equiv.) was added as a surfactant followed by another 15 min of sonication to complete the process of micelle formation. The water was evaporated in a flask with a septum and needle fitted in a vacuum oven overnight at 50 °C to leave a thin film. A small sample was removed for dynamic light scattering (DLS) measurements. For the preparation of samples for relaxometry measurements, the thin film was rehydrated with Milli-Q water (1 mL), sonicated for 15 min and passed through a 200 nm PTFE filter. The terbium(III) concentrations were analyzed by TXRF before relaxometric measurements.

Acknowledgments

L. V. E. and S. L. thank Fabian Rouffiange for his help, the French Community of Belgium for support through ARC programs (AUWB-2010-10/15-UMONS-5), the Fonds National de la Recherche Scientifique (FNRS), the Belgian Science Policy (UIAP VII program), for support and sponsorship concerted by COST Actions (D38 and TD1004), the European Network of Excellence EMIL (European Molecular Imaging Laboratories) program (LSCH-2004-503569), and the Center for Microscopy and Molecular Imaging (CMMI), supported by the European Regional Development Fund and the Walloon Region.

[1] E. Debroye, T. N. Parac-Vogt, *Chem. Soc. Rev.* **2014**, *43*, 8178–8192.
[2] J. C. Hebden, S. R. Arridge, D. T. Delpy, *Phys. Med. Biol.* **1997**, *42*, 825–840.

[3] P. Caravan, J. J. Ellison, T. J. McMurry, R. B. Lauffer, *Chem. Rev.* **1999**, *99*, 2293–2352.
[4] a) F. Hu, *Nanoscale* **2012**, *4*, 6235; b) S. L. Jeon, M. K. Chae, E. J. Jang, C. Lee, *Chem. Eur. J.* **2013**, *19*, 4217–4222; c) F. Ye, *Contrast Media Mol. Imaging* **2012**, *7*, 460–468; d) S. Soenen, *Contrast Media Mol. Imaging* **2009**, *4*, 207–219; e) H. B. Na, I. C. Song, T. Hyeon, *Adv. Mater.* **2009**, *21*, 2139–3148.
[5] a) A. J. L. Villaraza, A. Bumb, M. W. Briechbiel, *Chem. Rev.* **2010**, *110*, 2921–2959; b) P. Lebdušková, J. Kotek, P. Hermann, L. Vander Elst, R. N. Muller, I. Lukeš, J. A. Peters, *Bioconjugate Chem.* **2004**, *15*, 881–889; c) C.-H. Huang, K. Nwe, A. A. Zaki, M. W. Brechbiel, A. Tsourkas, *ACS Nano* **2012**, *6*, 9419–9424; d) Y. Li, M. Beija, S. Laurent, L. Vander Elst, R. N. Muller, H. T. T. Duong, A. B. Lowe, T. P. Davis, C. Boyer, *Macromolecules* **2012**, *45*, 4199–4204; e) K. Luo, G. Lui, W. She, Q. Wang, G. Wang, B. He, H. Ai, Q. Gong, B. Song, Z. Gu, *Biomaterials* **2011**, *32*, 7951–7960.
[6] a) M. Zhen, J. Zheng, L. Ye, S. Li, C. Jin, K. Li, D. Qiu, H. Han, C. Shu, Y. Yang, C. Wang, *ACS Appl. Mater. Interfaces* **2012**, *4*, 3724–3729; b) T. N. Parac-Vogt, K. Kimpe, S. Laurent, L. Vander Elst, C. Burtea, F. Chen, R. N. Muller, Y. C. Ni, A. Verbruggen, K. Binnemans, *Chem. Eur. J.* **2005**, *11*, 3077–3086; c) P. Caravan, *Acc. Chem. Res.* **2009**, *42*, 851–862; d) C. Henoumout, V. Henrotte, S. Laurent, L. Vander Elst, R. N. Muller, K. Binnemans, *J. Inorg. Biochem.* **2008**, *102*, 721–730.
[7] a) F. Kielar, L. Tei, E. Terreno, M. Botta, *J. Am. Chem. Soc.* **2010**, *132*, 7839–7837; b) T. N. Parac-Vogt, K. Kimpe, S. Laurent, C. Piérart, L. Vander Elst, R. N. Muller, K. Binnemans, *Eur. J. Inorg. Chem.* **2004**, 3538–3543; c) C. Vanasschen, N. Bouslimani, D. Thonon, J. F. Desreux, *Inorg. Chem.* **2011**, *50*, 8949–8958.
[8] a) A. Louie, *Chem. Rev.* **2010**, *110*, 3149–3195; b) L. Frullano, T. J. Meade, *J. Biol. Inorg. Chem.* **2007**, *12*, 939–949; c) D. Jańczewski, Y. Zhang, G. K. Das, D. K. Yi, P. Padmanabhan, K. K. Bhakoo, T. T. Y. Tan, S. T. Selvan, *Microsc. Res. Tech.* **2011**, *74*, 568–576.
[9] a) C. Bernhard, C. Goze, Y. Rousselin, F. Denat, *Chem. Commun.* **2010**, *46*, 8267–8269; b) A. Keliris, T. Ziegler, R. Mishra, R. Pohmann, M. G. Sauer, K. Ugurbil, J. Engelmann, *Bioorg. Med. Chem.* **2011**, *19*, 2529–2540.
[10] a) T. Koullourou, L. S. Natrajan, H. Bhavar, S. J. A. Pope, J. H. Feng, J. Narvainen, R. Shaw, E. Scales, R. Kauppinen, A. M. Kenwright, S. Faulkner, *J. Am. Chem. Soc.* **2008**, *130*, 2178–2179; b) G. Dehaen, S. V. Eliseeva, K. Kimpe, S. Laurent, L. Vander Elst, R. N. Muller, W. Dehaen, K. Binnemans, T. N. Parac-Vogt, *Chem. Eur. J.* **2012**, *18*, 293–302; c) G. Dehaen, S. V. Eliseeva, P. Verwilst, S. Laurent, L. Vander Elst, R. N. Muller, W. Deborggraeve, K. Binnemans, T. N. Parac-Vogt, *Inorg. Chem.* **2012**, *51*, 8775–8783; d) E. Debroye, G. Dehaen, S. V. Eliseeva, S. Laurent, L. Vander Elst, R. N. Muller, K. Binnemans, T. N. Parac-Vogt, *Dalton Trans.* **2012**, *41*, 10549–10556.
[11] a) N. Kamaly, T. Kalber, G. Kenney, J. Bell, M. Jorgensen, A. Miller, *Org. Biomol. Chem.* **2010**, *8*, 201–211; b) S. J. Soenen, G. V. Velde, A. Ketkar-Atre, U. Himmelreich, M. D. Cuyper, *Wiley Interdiscip. Rev. Nanomed. Nanobiotechnol.* **2011**, *3*, 197–211.
[12] W. J. Rieter, J. S. Kim, K. M. L. Taylor, H. An, W. Lin, T. Tarrant, W. Lin, *Angew. Chem. Int. Ed.* **2007**, *46*, 3680–3682; *Angew. Chem.* **2007**, *119*, 3754.
[13] a) P. Howes, M. Green, A. Bowers, D. Parker, G. Varma, M. Kallumadil, M. Hughes, A. Warley, A. Brain, R. Botnar, *J. Am. Chem. Soc.* **2010**, *132*, 9833–9842; b) S. Ronchi, M. Colombo, P. Verderio, S. Mazzucchelli, F. Corsi, C. D. Palma, R. Allevi, E. Clementi, D. Prosperi, *AIP Conf. Proc.* **2010**, *1275*, 102–105; c) D. Bhattacharya, M. Das, D. Mishra, I. Banerjee, S. K. Sahu, T. K. Maiti, P. Pramanik, *Nanoscale* **2011**, *3*, 1653–1662; d) Y. Chen, H. Chen, S. Zhang, F. Chen, L. Zhang, J. Zhang, M. Zhu, H. Wu, L. Guo, J. Feng, J. Shi, *Adv. Funct. Mater.* **2011**, *21*, 270–278.
[14] a) E. Debroye, M. Ceulemans, L. Vander Elst, S. Laurent, R. N. Muller, T. N. Parac-Vogt, *Inorg. Chem.* **2014**, *53*, 1257–1259; b) A. Boulay, C. Deraeve, L. Vander Elst, N. Leygue, O. Maury, S. Laurent, R. N. Muller, B. Mestre-Voegtlé, C. Picard, *Inorg. Chem.* **2015**, *54*, 1414–1425.
[15] E. Debroye, S. V. Eliseeva, S. Laurent, L. Vander Elst, R. N. Muller, T. N. Parac-Vogt, *Dalton Trans.* **2014**, *43*, 3589–3600.
[16] a) E. Debroye, S. Laurent, L. Vander Elst, R. N. Muller, T. N. Parac-Vogt, *Chem. Eur. J.* **2013**, *19*, 16019–16028; b) M. Harris, S. Carron, L. Vander Elst, S. Laurent, R. N. Muller, T. N. Parac-Vogt, *Chem. Commun.* **2015**, *51*, 2984–2986.
[17] S. Laurent, T. N. Parac-Vogt, K. Kimpe, C. Thirifays, K. Binnemans, R. N. Muller, L. Vander Elst, *Eur. J. Inorg. Chem.* **2007**, 2061–2067.
[18] E. Debroye, S. Laurent, L. Vander Elst, R. N. Muller, T. N. Parac-Vogt, *Chem. Eur. J.* **2013**, *19*, 16019–16028.
[19] H. Onishi, K. Sekine, *Talanta* **1972**, *19*, 473–478.
[20] A. Beeby, I. M. Clarkson, R. S. Dickins, S. Faulkner, D. Parker, L. Royle, A. S. d. Sousa, J. A. G. Williams, M. Woods, *J. Chem. Soc. Perkin Trans. 2* **1999**, 493–504.
[21] a) I. Hemmilä, S. Dakubu, V.-M. Mukkala, H. Siitari, T. Lövgren, *Anal. Biochem.* **1984**, *137*, 335–343; b) I. Hemmilá, V.-M. Mukkala, *Crit. Rev. Clin. Lab. Sci.* **2001**, *38*, 441–519; c) J. A. Keelan, J. T. France, P. M. Barling, *Clin. Chem.* **1987**, *33*, 2292–2295; d) I. Hemmilä, V. Laitala, *J. Fluoresc.* **2005**, *15*, 529–542.
[22] a) L. Vander Elst, A. Roch, P. Gillis, S. Laurent, F. Botteman, J. W. M. Bulte, R. N. Muller, *Magn. Reson. Med.* **2002**, *47*, 1121–1130; b) P. Caravan, M. T. Greenfield, J. W. M. Bulte, *Magn. Reson. Med.* **2001**, *46*, 917–922.
[23] a) S. Viswanathan, Z. Kovacs, K. N. Green, S. J. Ratnakar, A. D. Sherry, *Chem. Rev.* **2010**, *110*, 2960–3018; b) J. A. Peters, J. Huskens, D. J. Raber, *Prog. Nucl. Magn. Reson. Spectrosc.* **1996**, *28*, 283–350.
[24] A. Accardo, D. Tesauro, L. Aloj, C. Pedone, G. Morelli, *Coord. Chem. Rev.* **2009**, *253*, 2193–2213.

Received: March 23, 2015
Published Online: June 23, 2015

